Int J Fract (2022) 238:71–87
https://doi.org/10.1007/s10704-022-00654-y

ORIGINAL PAPER

Finite deformation field near the tip of a Blatz–Ko wedge bonded to a rigid substrate

Chung-Yuen Hui · Bangguo Zhu · Matteo Ciccotti

Received: 9 February 2022 / Accepted: 27 June 2022 / Published online: 29 July 2022

Abstract Sharp corners or wedges are common in everyday structures. Depending on the internal angle θ_0 of the wedge, severe stress concentration can occur. Linear elasticity predicts that when an incompressible elastic wedge is bonded to a rigid substrate and subjected to plane strain deformation, the stresses at the wedge tip has a power law singularity if $\theta_0 > 45°$. For some θ_0 and for compressible wedges, the stresses are not only singular but oscillate infinitely rapidly. Here we show that these results are no longer true if large deformation is taken into consideration. Specifically, we determine the asymptotic fields near a tip of a Blatz–Ko wedge and found that the stress field has no power singularity for $\theta_0 \leq 90°$. Furthermore, the power law singularity of the stress field differs from those predicted by linear elasticity and there are no oscillations. For sufficiently low compressibility, it is possible to obtain higher order terms of the asymptotic series—analogous to William's expansion in linear theory. Our asymptotic results are validated by finite element calculations. We also studied the wedge tip field for the borderline case of a 90° wedge. For this case, the stress singularity is found to be at most logarithmic.

Keywords Finite strain · Hyperelasticity · Compressible · Wedge · Asymptotic analysis · Finite element analysis

Chung-Yuen Hui and Bangguo Zhu have contributed equally to this work.

Supplementary Information The online version contains supplementary material available at https://doi.org/10.1007/s10704-022-00654-y.

C.-Y. Hui · B. Zhu (✉)
Field of Theoretical and Applied Mechanics, Department of Mechanical and Aerospace Engineering, Cornell University, Ithaca, NY 14853, USA
e-mail: bz347@cornell.edu

C.-Y. Hui
Global Station for Soft Matter, Global Institution for Collaborative Research and Education (GI-CoRE), Hokkaido University, Sapporo 001-0021, Japan

M. Ciccotti
Sciences et lngénierie de la Matière Molle, CNRS UMR 7615, École Supérieure de Physique et de Chimie Industrielles de la Ville de Paris (ESPCI), ParisTech, PSL Research Univeristy, 10 rue Vauquelin, 75231 Paris cedex 05, France

1 Introduction

Wedge shaped corners are ubiquitous in structures. For example, the use of patches bonded with structural adhesives is increasingly widespread in applications such as aircrafts, cars and other transport related applications. However, adhesively bonded patches have problems of stress concentration at the corners where crack initiation is prone to occur leading to the

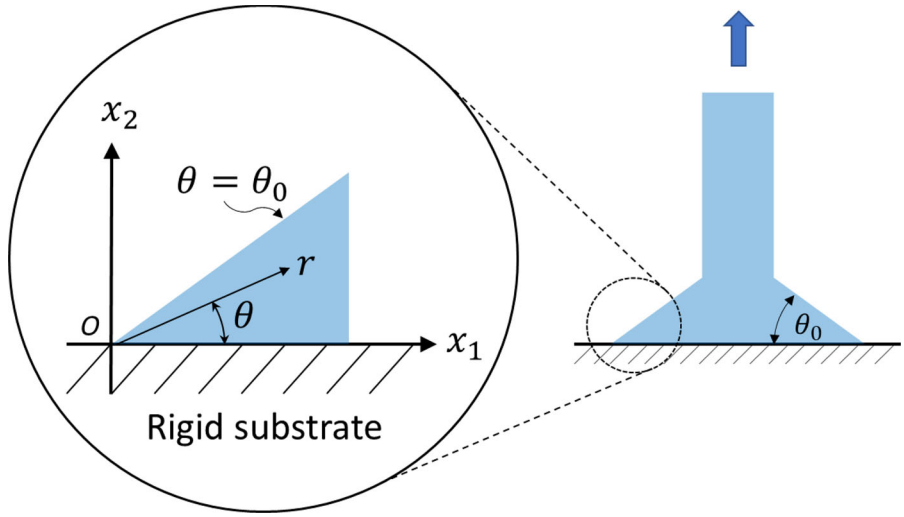

Fig. 1 Figure inside circle shows local geometry of wedge for asymptotic analysis in the un-deformed reference configuration. The lower edge of the wedge $\theta = 0$ is bonded to the rigid substrate. Its edge at $\theta = \theta_0$ is traction free. We consider plane strain deformation where the out of plane displacement is identically zero and the fields are independent of x_3. The out of plane coordinate x_3 is not shown. Geometry in the simulation of Aksak et al. (2014) is shown on the right

debonding of the patch. Such stress concentration can be reduced by tapering the surfaces of the patch, but tapering the adhesive is also an option (Marques and da Silva 2008). In nature, small animals can achieve strong and robust adhesion with small patches such as the suction cups of octopus (Tramacere et al. 2014), the sticky fibrils of mussels (Ornes 2013), vine tree and gecko feet (Arzt et al. 2003). This strategy employed by nature has motivated the development of bioinspired structured adhesive surfaces (Gorb et al. 2006; Kim and Sitti 2006; Jagota and Hui 2011) to control adhesion and friction. These surfaces are typically made of an array of soft elastomeric fibers with shear modulus on the order of 1 MPa. Adhesion is typically measured against a rigid smooth surface such as glass. Experimentally and theoretically, it has been found that the shape of fiber tip can significantly affect contact and adhesion (del Campo et al. 2007; Spuskanyuk et al. 2008). Using finite element (FE) simulations based on linear elasticity and a cohesive zone model for debonding, Aksak et al. (2014) have found that wedge shape fiber tips (see Fig. 1 insert) with an internal angle of $\theta_0 = 45°$ optimize the pull-off stress per unit contact area of a single fiber.[1]

[1] There are other geometrical factors such as the aspect ratio of the fiber which control the optimal pull-off force.

Motivated by these applications, we study the generic problem in Fig. 1 where a wedge in an elastic solid is bonded to a rigid substrate; depending on the internal angle θ_0 of the wedge, severe stress concentration is known to occur. Williams (1952) was the first to study the stress singularity near a wedge tip in a linear isotropic elastic solid. He studied various sets of boundary conditions (BC) on the radial edges of a wedge in thin elastic plates under extension. William's ideas were later extended to wedges between dissimilar linear elastic materials, including anisotropic solid wedges (Bogy 1968; Hein and Erdogan 1971; Dempsey and Sinclair 1979). The main goal of these papers is to characterize the singular deformation and stress fields near the tip of elastic wedges. The use of these asymptotic fields to predict failure in applications can be found in Dunn et al. (1997a, b) and Leguillon (2002). The idea is that these wedge singular fields fully characterize the stress and strain state near the wedge tip, hence their amplitude can be used as a loading parameter to determine crack initiation.

Here we note that all the above works are based on linearized theory of elasticity where both the kinematics and material behavior are linear. As a result, they generally work for hard and stiff solids. For soft materials such as adhesives and elastomers, the deformation near the wedge tip can be sufficiently

large to violate the small strain assumption. Because of this, it is expected that there can be significant differences between the prediction of small strain and large deformation theory. For crack problems, these differences have been studied by Knowles and Steinberg (1973, 1974, 1983), Stephenson (1982), Geubelle and Knauss (1994a, b, c) and Gao (1990). The finite strain crack tip fields exhibit characteristics that are drastically different from those of the linear elastic fracture mechanics solution, see Long and Hui (2015) for a detailed review. On the other hand, there are much fewer works on the behavior of the stress field near the tip of hyper-elastic wedges. Most of these works focus on *homogeneous* hyper-elastic solids (Mansouri et al. 2016). However, in many applications, such as those mentioned above, the wedge is bonded to very stiff substrates. This motivates us to consider the stress and deformation field near the tip of a hyper-elastic wedge (see Fig. 1) that is bonded to a rigid substrate.

We consider plane strain deformation. The wedge in this work is a compressible hyper-elastic solid proposed by Blatz and Ko (1962). This material model was used by Lengyel et al. (2014) to study the asymptotic behavior of an interface crack between a compressible hyper-elastic solid and a rigid substrate which corresponds to $\theta_0 = \pi$. Here we study the existence of singular fields near the wedge tip and, if they exist, how they depend on the wedge angle. These asymptotic solutions are validated by FE simulations.

The plan of this paper is as follows. In Sect. 2 we review linear wedge asymptotic theory that is relevant to this work. In Sect. 3 we introduce the finite strain model for the wedge problem. The asymptotic solution for $\pi > \theta_0 > \pi/2$ is given in Sect. 4. In contrast to linear theory, where the transition between singular and non-singular tip solution occurs at $\theta_0 \approx \pi/4$ for solids with low compressibility, we found that there is no power-law singular solution for $\theta_0 \leq \pi/2$. In Sect. 5, we check our asymptotic solution against FE simulations. In Sect. 6, we study the transition case where $\theta_0 = \pi/2$. Summary and discussion are given in Sect. 7.

2 Linearized theory of wedge tip fields (LTW)

To gain perspective, we summarize results based on linearized theory of elasticity that are relevant to this study. Williams (1952) was the first to study the stress singularity near a wedge tip in a linear isotropic elastic solid. He studied various set of boundary conditions (BC) on the radial edges of a wedge in thin plates under extension. The BC that is relevant to this work is a clamped/free boundary. The clamped edge represents the rigid substrate in our problem (see Fig. 1 for geometry). We note here that William's solution is for plane stress deformation. However, the solution of plane strain problems can be readily obtained from the plane stress solution by a simple transformation of elastic constants (Muskhelishvili 1977). The results below are modified for plane strain deformation.

Williams (1952) showed that the in-plane asymptotic stress field $\tau_{\alpha\omega}$, with respect to a polar coordinate system (r, θ) with origin at the wedge tip, has the form

$$\tau_{\alpha\omega} = r^{m-1}\hat{\tau}_{\alpha\omega}(\theta, \theta_0, \nu, A_1, A_2), \quad r \to 0 \tag{1}$$

where A_1 and A_2 are loading parameters that controls the intensity of the stress field, ν is the Poisson's ratio of the elastic wedge and $\hat{\tau}_{\alpha\omega}$ are linear homogeneous functions of A_1 and A_2. The parameters A_1 and A_2 cannot be determined from asymptotic analysis; they depend on the geometry of the structure and the manner of loading. In (1), m is the *singularity index* which can be complex. Typically, one requires that the real part of m to be greater than *0* so that the displacement field is bounded. Here we note the following:

- m is a function of the wedge angle θ_0 and the Poisson's ratio ν. Specifically, the relation between m and θ_0 for plane strain deformation is given by the transcendental equation:

$$m^2 \sin^2\theta_0 - 4(1-\nu)^2 + (3-4\nu)\sin^2(m\theta_0) = 0. \tag{2}$$

- Note that the singularity index depends only on the Poisson's ratio and the wedge angle and is otherwise independent of material properties such as the shear modulus.
- m can be a complex number for some wedge angles, i.e., $m = m_1 + im_2$ where $i = \sqrt{-1}$. For this case, the stress can be obtained by taking the real or imaginary part of (1). Since

$$r^{m-1} = r^{m_1-1}[\cos(m_2 \ln r) + i \sin(m_2 \ln r)], \tag{3}$$

the stresses oscillate infinitely rapidly as r approaches the wedge tip if $m_2 \neq 0$. Such oscillatory behavior is well documented for interface cracks in bi-material systems (England 1965; Rice and Sih 1965). Knowles and Sternberg (1983) showed that such oscillatory behavior arises from the linearization of the field equations; by carrying out asymptotic analysis of the nonlinear field equations governing an interface crack between two compressible neo-Hookean sheets, they found that the crack faces open smoothly, and the stress field has no oscillatory behavior.

Figure 2 plots the numerical solution of (2) against θ_0 for $\nu = 0.33$, 0.45 and 0.5 (incompressible solid). For the case of $\nu = 0.5$, m is *real* for all angles. However, this is not the case for $\nu < 0.5$, where complex root can exist. Note that Re m versus θ_0 has a cusp at some m, to the left of this cusp, m is real while m is complex to its right. The solid black line in Fig. 2 is the result of the finite strain theory (details are given in Sects. 3–4). In finite strain theory there are no complex roots and stresses *has no power singularity* for $\theta \leq \pi/2$(see below for details).

We highlight the following results of the linear theory for comparison purposes:

- The stress field has a power singularity and is unbounded if Re$m < 1$. It is bounded when Re$m \geq 1$.
- For an incompressible solid loaded in plane strain, m is always real and $m = 1$ at $\theta_0 = \pi/4$ or 45 degrees. Thus, the stress and strain fields are bounded and continuous when $\theta_0 \leq \pi/4$. Note that this is consistent with the result of Aksak et al. (2014), suggesting that the optimal pull-off force occurs when the singular fields near the wedge tip is eliminated.
- For compressible solids, m is complex for wedge angles, $\theta_0 > \theta_c(\nu)$, where $\theta_c(\nu)$ denotes the critical angle where the transition from real to complex root occurs. A plot of $\theta_c(\nu)$ versus ν is given in the SI. For wedge angles greater than $\theta_c(\nu)$, the stress field is singular and oscillates infinitely rapidly at the tip. We shall see later that this oscillatory behavior is absent in large deformation.
- For $\theta_0 = \pi/2$, $m = m_1 < 1$ for all $\nu > 0$, hence the stress has a non-oscillatory singularity r^{m-1}. As shown in Fig. 3, the singularity index is found to decrease with increasing ν; hence the stress is most singular when $\nu = 1/2$. We shall see later that the large deformation solution does not admit a power law singularity when $\theta_0 = \pi/2$. Instead, a much weaker logarithmic singularity is found for this case.

A brief discussion of transition between the linear and nonlinear asymptotic solutions are given in the SI.

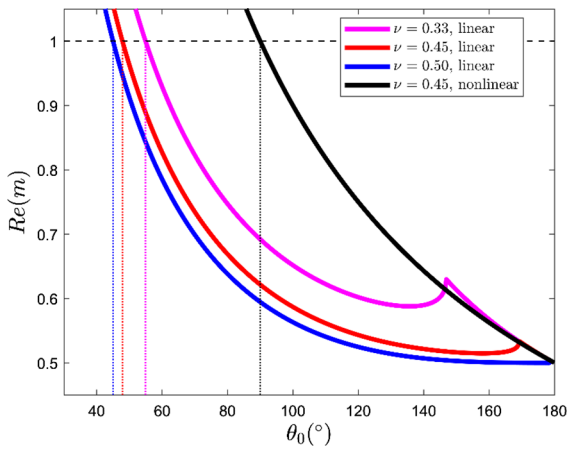

Fig. 2 The real part of the singularity index m in the linear theory for $\nu = 0.33$, 0.45 and 0.5

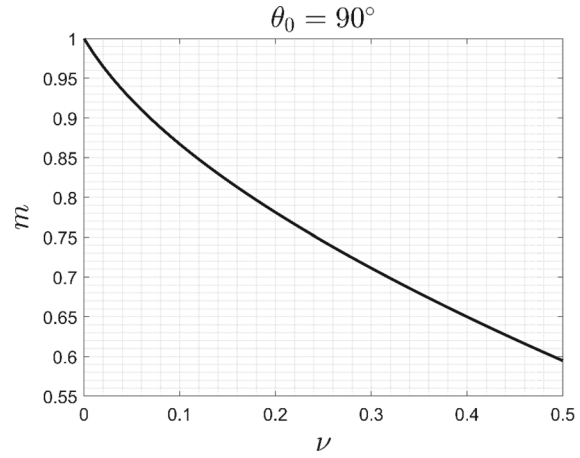

Fig. 3 The singularity index for $\theta_0 = \pi/2$ as a function of the Poisson's ratio ν. For this angle m is always real and less than *1* except at $\nu = 0$, indicating that the stress has power singularity of the form r^{m-1} for $\nu > 0$

3 Finite strain model of wedge tip fields

3.1 Problem formulation and geometry

The geometry consists of a compressible hyper-elastic wedge of angle θ_0 bonded to the surface of a rigid substrate (see Fig. 1). A material point in the reference undeformed configuration is denoted by its Cartesian coordinates x_i (i = 1, 2, 3). We consider plane strain deformation where all field quantities are independent of the out of plane coordinate x_3. In the following we will use Greek indices to denote in plane coordinates, e.g., x_α,$\alpha = 1, 2$. Details on plane strain deformation were given by Stephenson (1982). Here we summarize the basic equations.

In plane strain, the out of plane deformation is exactly zero, so deformation can be represented by a 2D deformation gradient tensor $\boldsymbol{F}$ with Cartesian components $F_{\alpha\omega} = \partial y_\alpha/\partial x_\omega$, where $y_\alpha = x_\alpha + u_\alpha(x_1, x_2)$ is the deformed coordinates of the material point and u_α is its displacement in the α direction. The strain energy density function W for an isotropic hyper-elastic solid undergoing plane strain deformation is a function of two invariants $I = tr(\boldsymbol{F}\boldsymbol{F}^T)$ and $J = \det \boldsymbol{F}$. The 1st Piola or nominal stress tensor $\boldsymbol{P}$ is related to $W(I, J)$ by

$$\boldsymbol{P} = 2\frac{\partial W}{\partial I}\boldsymbol{F} + J\frac{\partial W}{\partial J}\boldsymbol{F}^{-T}. \tag{4}$$

The true or Cauchy stress tensor $\boldsymbol{\tau}$ is related to the 1st Piola stress tensor by

$$\boldsymbol{\tau} = J^{-1}\boldsymbol{P}\boldsymbol{F}^T \tag{5}$$

3.2 Material model

We consider a compressible hyper-elastic solid proposed by Blatz and Ko (1962). As noted in the introduction, this material model was used by Lengyel et al. (2014) to study the asymptotic behavior of an interface crack between a compressible hyper-elastic solid and a rigid substrate ($\theta_0 = \pi$). The 2D plane strain energy density function is given by

$$W = \frac{\mu}{2}(I - 2) + \frac{\mu}{2\beta}\left(J^{-2\beta} - 1\right), \tag{6}$$

where μ is the small strain shear modulus. The dimensionless constant β is the compressibility factor, it is related to the small strain Poisson's ratio v by $\beta = v/(1 - 2v) \geq 0$. This relation indicates that large β corresponds to low compressibility. For many soft materials, such as elastomers and gels, the resistance to shear is much smaller than the resistance to compression, resulting in $\beta >> 1$. For example, an elastomer used in many applications is Polydimethylsiloxane (PDMS). The Poisson's ratio of PDMS (Sylgard 184, from Dow Chemical Company) was reported by Müller et al. (2019) to be 0.495, which corresponds to $\beta = 49.5$. The in-plane nominal stress tensor components $P_{\alpha\beta}$ are obtained using (4) and (6), they are

$$\begin{aligned} &P_{11} = \mu\left[F_{11} - J^{-2\beta-1}F_{22}\right],\ P_{12} = \mu\left[F_{12} + J^{-2\beta-1}F_{21}\right] \\ &P_{21} = \mu\left[F_{21} + J^{-2\beta-1}F_{12}\right],\ P_{22} = \mu\left[F_{22} - J^{-2\beta-1}F_{11}\right] \end{aligned} \tag{7a–d}$$

The in-plane true stress components $\tau_{\alpha\omega}$ are evaluated using (7a–d) and (5), they are:

$$\begin{aligned} \tau_{11} &= J^{-1}\mu\left\{\left[F_{11}^2 + F_{12}^2\right] - J^{-2\beta}\right\} \\ \tau_{12} = \tau_{21} &= J^{-1}\mu[F_{11}F_{21} + F_{12}F_{22}] \\ \tau_{22} &= J^{-1}\mu\left\{\left[F_{21}^2 + F_{22}^2\right] - J^{-2\beta}\right\} \end{aligned} \tag{8a – d}$$

3.3 Equilibrium

In the absence of body forces,[2] the equilibrium equations in the reference configuration are

$$\nabla_x \cdot \boldsymbol{P} = 0 \tag{9}$$

Substituting (7a–d) into (9), the equilibrium equations are:

$$\begin{aligned} &\nabla_x^2 y_1 + (2\beta + 1)J^{-2(\beta+1)}(\nabla_x J \times \nabla_x y_2) \cdot \boldsymbol{E}_3 = 0 \\ &\nabla_x^2 y_2 - (2\beta + 1)J^{-2(\beta+1)}(\nabla_x J \times \nabla_x y_1) \cdot \boldsymbol{E}_3 = 0 \end{aligned} \tag{10a, b}$$

where $\boldsymbol{E}_3$ is the unit vector in the out of plane direction and ∇_x^2 is the 2D Laplacian in reference coordinates. As in Sect. 2, we use the polar coordinates (r, θ) in the reference configuration as independent variables:

$$x_1 = r\cos\theta, \quad x_2 = r\sin\theta \tag{11}$$

[2] As long as the body forces are bounded, they have no effect on the leading singular behavior of the fields.

Using r, θ as independent variables, the equilibrium Eqs. (10a, b) become:

$$\frac{1}{r}\frac{\partial}{\partial r}\left(r\frac{\partial u_1}{\partial r}\right)+\frac{1}{r^2}\frac{\partial^2 u_1}{\partial \theta^2}+\frac{(2\beta+1)J^{-2(\beta+1)}}{r}\left[\frac{\partial J}{\partial r}\frac{\partial y_2}{\partial \theta}-\frac{\partial y_2}{\partial r}\frac{\partial J}{\partial \theta}\right]=0$$

$$\frac{1}{r}\frac{\partial}{\partial r}\left(r\frac{\partial y_2}{\partial r}\right)+\frac{1}{r^2}\frac{\partial^2 y_2}{\partial \theta^2}-\frac{(2\beta+1)J^{-2(\beta+1)}}{r}\left[\frac{\partial J}{\partial r}\left(-r\sin\theta+\frac{\partial u_1}{\partial \theta}\right)-\left(\cos\theta+\frac{\partial u_1}{\partial r}\right)\frac{\partial J}{\partial \theta}\right]=0 \tag{12a, b}$$

where J is

$$J=\frac{1}{r}\left[\left(\cos\theta+\frac{\partial u_1}{\partial r}\right)\frac{\partial y_2}{\partial \theta}-\frac{\partial y_2}{\partial r}\left(-r\sin\theta+\frac{\partial u_1}{\partial \theta}\right)\right] \tag{12c}$$

These equations are the same as in Lengyel et al. (2014). However, it must be noted that Lengyel et al. (2014) used the symbol x_α to denote deformed coordinates. Also, instead of using y_1, y_2 as the dependent variables, which is typically adopted in nonlinear field analysis, we use u_1, y_2 as the dependent variables. Since $y_1 = u_1 + r\cos\theta$, the usage of u_1 as independent variable made the BC $y_1 = r$ on the interface homogeneous (see (13a) below).

3.4 Boundary conditions (BC) for asymptotic analysis

We consider perfect bonding, hence the displacements on the interface $\theta = 0, r > 0$ are identically zero, i.e.,

$$u_1(\theta=0, r>0)=0,\ y_2(\theta=0, r>0)=0 \tag{13a, b}$$

The edge of the wedge at $\theta = \theta_0, r > 0$ is traction free, i.e.,

$$\boldsymbol{P}\cdot\boldsymbol{N}=0 \tag{14}$$

where $\boldsymbol{N}$ is the unit normal vector to the free edge. Using (7a–d), the BC (14) can be written in terms of u_1, y_2 as:

$$-\sin\theta_0+\frac{1}{r}\frac{\partial u_1}{\partial \theta}+J^{-2\beta-1}\frac{\partial y_2}{\partial r}=0 \quad \text{at } \theta=\theta_0$$

$$\frac{1}{r}\frac{\partial y_2}{\partial \theta}-J^{-2\beta-1}\left(\cos\theta_0+\frac{\partial u_1}{\partial r}\right)=0 \quad \text{at } \theta=\theta_0 \tag{15a, b}$$

4 Asymptotic analysis of wedge tip fields

4.1 Asymptotic analysis

In this work we assume $\theta_0 < \pi$ since the crack case where $\theta_0 = \pi$ was solved by Lengyel et al. (2014). We consider the expansion near $r = 0$,

$$u_1 = r^{m_1}v_1(\theta)+o(r^{m_1})$$
$$y_2 = r^{m_2}v_2(\theta)+o(r^{m_2}) \quad 0<m_\alpha<1 \tag{16a, b}$$

The condition $0 < m_\alpha < 1$ enforces continuity of displacements but allows for singular stresses and displacement gradients. Substituting (16a, b) into (12c), we found

$$\begin{aligned} J &\sim \frac{1}{r}\left[\left(\cos\theta+m_1r^{m_1-1}v_1\right)r^{m_2}v_2'\right.\\ &\quad \left.-m_2r^{m_2-1}v_2\left(-r\sin\theta+r^{m_1}v_1'\right)\right]\\ &\sim r^{m_1+m_2-2}\left[m_1v_1v_2'-m_2v_2v_1'\right] \end{aligned} \tag{17}$$

Equation (16a) implies that the Laplacian term in (12a) is

$$\nabla_x^2 u_1 \sim r^{m_1-2}\left(v_1''+m_1^2v_1\right), \tag{18a}$$

while the 3rd term in (12a) (we will call this the *nonlinear* term) is

$$\frac{J^{-2(\beta+1)}}{r}\left[\frac{\partial J}{\partial r}\frac{\partial y_2}{\partial \theta}-\frac{\partial y_2}{\partial r}\frac{\partial J}{\partial \theta}\right]\sim r^{-2(\beta+1)(m_1+m_2-2)}r^{2m_2-2}r^{m_1-2} \tag{18b}$$

Using (18a, b), the ratio of the nonlinear to the Laplace term is seen to vanish as r goes to zero, i.e.,

$$r^{-2(\beta+1)(m_1+m_2-2)}r^{2m_2-2}=r^{-2(\beta+1)(m_1-1)}r^{-2\beta(m_2-1)}\to 0, \tag{19}$$

where we have used $0 < m_\alpha < 1$. Hence the nonlinear term (18b) can be neglected and the leading order behavior of (12a) is determined by (18a), i.e.,

$$v_1'' + m_1^2 v_1 = 0. \tag{20}$$

The solution of (20) that satisfies the BC (13a) is

$$v_1 = a_1 \sin(m_1\theta), \tag{21}$$

where a_1 is an arbitrary constant. To satisfy the traction free boundary condition (15a), we note that the third term in (15a) is of order

$$\begin{aligned} J^{-2\beta-1}\frac{\partial y_2}{\partial r} &\sim r^{-(2\beta+1)(m_1+m_2-2)} r^{m_2-1} \\ &= r^{-(2\beta+1)(m_1-1)} r^{-2\beta(m_2-1)}. \end{aligned} \tag{22}$$

Comparing the order of each term in (15a) is of order (15a), we have

$$\underbrace{-\sin\theta_0}_{O(1)} + \underbrace{\frac{1}{r}\frac{\partial u_1}{\partial\theta}}_{O(r^{m_1-1})} + \underbrace{J^{-2\beta-1}\frac{\partial y_2}{\partial r}}_{O(r^{-(2\beta+1)(m_1-1)} r^{-2\beta(m_2-1)})} = 0\,. \tag{23}$$

The dominant term in (23) is clearly $\frac{1}{r}\frac{\partial u_1}{\partial\theta}$, hence, to leading order, the BC (15a) becomes:

$$\begin{aligned} \left.\frac{\partial u_1}{\partial\theta}\right|_{\theta_0} &= 0 \Rightarrow v_1'(\theta_0) = 0 \Rightarrow \cos(m_1\theta_0) = 0 \Rightarrow m_1 \\ &= \frac{\pi}{2\theta_0}. \end{aligned} \tag{24}$$

Equation (24) determines the singularity index for the horizontal displacement u_1. *Here we note the assumption that $m_1 < 1$ holds if and only if $\theta_0 > \pi/2$.*

We next consider the leading order solution of (12b), the Laplacian term is

$$\nabla^2 y_2 \sim r^{m_2-2}\left(v_2'' + m_2^2 v_2\right). \tag{25a}$$

The nonlinear term is:

$$\begin{aligned} &\frac{J^{-2(\beta+1)}}{r}\left[\frac{\partial J}{\partial r}\left(-r\sin\theta + \frac{\partial u_1}{\partial\theta}\right) - \left(\cos\theta + \frac{\partial u_1}{\partial r}\right)\frac{\partial J}{\partial\theta}\right] \\ &\sim r^{-2(\beta+1)(m_1+m_2-2)} r^{2m_1-2} r^{m_2-2}, \end{aligned} \tag{25b}$$

which goes to zero in comparison with the Laplacian term. Therefore,

$$v_2'' + m_2^2 v_2 = 0 \Rightarrow v_2 = a_2 \sin m_2\theta \tag{26}$$

where we have used the BC (13b). The same argument shows that the leading order behavior of (15b) is

$$\frac{\partial y_2}{\partial\theta} \sim 0 \quad \text{at } \theta = \theta_0 \Rightarrow \cos(m_2\theta_0) = 0. \tag{27}$$

Equation (27) implies that

$$m_2 = \frac{\pi}{2\theta_0} = m_1 \equiv m. \tag{28}$$

Thus, *the singularity index for u_1 and y_2 is equal*.

We need to recalculate J since the leading order term in (17), $\left[m_1 v_1 v_2' - m_2 v_2 v_1'\right] = m\left[v_1 v_2' - v_2 v_1'\right]$ *vanishes identically* [See (21) and (26)]. A simple calculation using [(17), upper equation] shows that

$$\begin{aligned} J &\sim \frac{1}{r}\left[\left(\cos\theta + a_1 m r^{m-1}\sin m\theta\right) a_2 r^m m\cos m\theta\right. \\ &\quad \left. - a_2 m r^{m-1}\sin m\theta(-r\sin\theta + a_1 m r^m\cos m\theta)\right] \\ &= a_2 m r^{m-1}\cos[(1-m)\theta] \end{aligned} \tag{29}$$

Comparing (29) with (17) shows that the leading order behavior of J has changed because $\left[m_1 v_1 v_2' - m_2 v_2 v_1'\right]$ *vanishes, it is now r^{m-1} instead of r^{2m-2}*. However, since $m < 1$, J is still unbounded as r goes to zero. Note J is non-zero inside and on the wedge boundaries since $\cos[(1-m)\theta] > 0$ in $0 \le \theta \le \theta_0$. However, because $\left[m_1 v_1 v_2' - m_2 v_2 v_1'\right]$ vanishes identically, J is now of order r^{m-1}, so we need to check that the Laplacian terms in (12a,b) still dominate the nonlinear term. This is indeed the case since

$$\begin{aligned} &\frac{J^{-2(\beta+1)}}{r}\left[\frac{\partial J}{\partial r}\frac{\partial y_2}{\partial\theta} - \frac{\partial y_2}{\partial r}\frac{\partial J}{\partial\theta}\right] \\ &\sim r^{-2(\beta+1)(m-1)} r^{m-1} r^{m-2} >> r^{m-2}, \end{aligned} \tag{30a}$$

$$\begin{aligned} &\frac{J^{-2(\beta+1)}}{r}\left[\frac{\partial J}{\partial r}\left(-r\sin\theta + \frac{\partial u_1}{\partial\theta}\right) - \left(\cos\theta + \frac{\partial u_1}{\partial r}\right)\frac{\partial J}{\partial\theta}\right] \\ &\sim r^{-2(\beta+1)(m-1)} r^{m-1} r^{m-2} >> r^{m-2}. \end{aligned} \tag{30b}$$

Thus, (21), (26), (28) are still valid provide that the leading behavior of J is given by (29).

4.2 Higher order terms

Our result in previous section shows that, in contrast to the linear theory where m is a function of the Poisson's ratio [see (2)], the singularity index m in the leading order solution of the finite strain theory *does not*

depend on the compressibility factor β [see (28)]. We show here that the effect of compressibility is manifested in higher order terms in the asymptotic expansion [see (43) below]. To see this, consider

$$u_1 = a_1 r^m \sin m\theta + r^{n_1} w_1(\theta) + o(r^{n_1})$$
$$y_2 = a_2 r^m \sin m\theta + r^{n_2} w_2(\theta) + o(r^{n_2}) \quad \text{where } n_\alpha \geq 1 \tag{31a, b}$$

Since the first terms in (31a, b) satisfy the Laplace equation exactly, we have

$$\nabla^2 u_1 \sim r^{n_1-2}\left(w_1'' + n_1^2 w_1\right)$$
$$\nabla^2 y_2 \sim r^{n_2-2}\left(w_2'' + n_2^2 w_2\right) \tag{32a, b}$$

The leading order of J is still given by (29), more precisely,

$$J = r^{m-1} a_2 m \cos[(1-m)\theta] + o\left(r^{m-1}\right) \tag{33}$$

Using (33) and (31a, b), the leading order behavior of the nonlinear term in (12a) is

$$\frac{1}{r}\left[\frac{\partial J}{\partial r}\frac{\partial y_2}{\partial \theta} - \frac{\partial y_2}{\partial r}\frac{\partial J}{\partial \theta}\right] \sim m^2(1-m)a_2^2 r^{m-1} r^{m-2}$$
$$(\cos m\theta \cos[(1-m)\theta] + \sin m\theta \sin[(1-m)\theta])$$
$$= (m-1)a_2^2 m^2 r^{m-1} r^{m-2} \cos\theta \tag{34}$$

Combining (34) and (33), the leading order behavior of the nonlinear term in (12a) is

$$J^{-2(\beta+1)} \frac{1}{r}\left[\frac{\partial J}{\partial r}\frac{\partial y_2}{\partial \theta} - \frac{\partial y_2}{\partial r}\frac{\partial J}{\partial \theta}\right]$$
$$= O(r^{2(\beta+1)(1-m)} r^{m-1} r^{m-2}) = O\left(r^{2\beta(1-m)-1}\right) \tag{35}$$

Let us first assume that $n_1 > 1$. If the nonlinear term is small in comparison with the Laplacian term as r goes to zero, then

$$n_1 - 2 < 2\beta(1-m) - 1 \Leftrightarrow n_1 < 1 + 2\beta(1-m). \tag{36}$$

Since $1/2 < m < 1$, for any fixed $\theta_0 > \pi/2$ (36) is true for sufficiently large β. Let us assume this is the case since we are mostly interested in solids with low compressibility, then the Laplacian term dominates which results in

$$w_1'' + n_1^2 w_1 = 0 \Rightarrow w_1 = b_1 \sin(n_1\theta). \tag{37}$$

Let us consider the boundary condition (15a). By (24), the term $\frac{1}{r}\frac{\partial u_1}{\partial \theta}$ in (15a) is of order $r^{n_1-1} w_1'$. However, it is impossible for this term to dominant (unless $\sin\theta_0 = \sin\pi = 0$, recall we exclude the crack case) since $n_1 > 1$ and this term vanishes as r goes to zero. The last term in the BC (15a) is

$$J^{-2\beta-1}\frac{\partial y_2}{\partial r} \sim r^{(2\beta+1)(1-m)} r^{m-1} = r^{(2\beta)(1-m)}, \tag{38}$$

which also goes to zero as r goes to zero since $m < 1$. By (36) this term is small compared with $\frac{1}{r}\frac{\partial u_1}{\partial \theta} \sim \frac{r^{n_1}}{r} w_1'$ as r goes to zero. Thus, the 1st term in the BC (15a) dominates and the BC (15a) cannot be satisfied. This means that it is not possible for $n_1 > 1$. The only choice is $n_1 = 1$. For this case (36) is always satisfied since m is less than 1, so the Laplacian term dominates and (32a) and (13b) implies that

$$w_1 = b_1 \sin\theta. \tag{39}$$

What about the BC (15a)? Using (38), the order of each term in (15a) is:

$$-\sin\theta_0 + b_1 \cos\theta_0 + \underbrace{J^{-2\beta-1}\frac{\partial y_2}{\partial r}}_{r^{2\beta(1-m)} \to 0} = 0 \Rightarrow b_1 = \tan\theta_0. \tag{40}$$

Hence the 2nd order solution for u_1 is $r\tan\theta_0 \sin\theta$, that is

$$u_1 = a_1 r^m \sin m\theta + r\tan\theta_0 \sin\theta + o(r). \tag{41}$$

Having determine the next order term for u_1, we turn to y_2. Using (29), the first order behavior of the nonlinear term in (12b) is:

$$\frac{J^{-2(\beta+1)}}{r}\left[\frac{\partial J}{\partial r}\left(-r\sin\theta + \frac{\partial u_1}{\partial \theta}\right) - \left(\cos\theta + \frac{\partial u_1}{\partial r}\right)\frac{\partial J}{\partial \theta}\right]$$
$$\sim r^{2(\beta+1)(1-m)} r^{2m-3}\{a_2 m \cos[(1-m)\theta]\}^{-2(1+\beta)}$$
$$a_1 a_2 (m-1) m^2 \cos\theta \tag{42}$$

Again, the Laplace term in (12b) is of order r^{n_2-2}, assuming it dominates (this requires β to be sufficiently large, exactly how large we shall see below), we must have

$$r^{n_2-2} >> r^{2(\beta+1)(1-m)} r^{2m-3} \Rightarrow n_2 < 2\beta(1-m) + 1 \tag{43}$$

Equation (43) implies that the linear term of the boundary condition (15b) is the dominant term, so:

$$\frac{1}{r}\frac{\partial y_2}{\partial \theta} \sim 0 \text{ at } \theta = \theta_0 \text{ and } y_2(\theta = 0) = 0 \tag{44}$$

Since $n_2 \geq 1$, the solution of the Laplacian (32b) is

$$b_2 r^{n_2} \sin n_2\theta, \quad n_2 = \frac{3\pi}{2\theta_0} \tag{45}$$

Thus,

$$y_2 = a_2 r^m \sin m\theta + b_2 r^{n_2} \sin n_2\theta + o(r^{n_2}) \tag{46}$$

To summarize, the asymptotic expansion of the deformed coordinates are:

$$\begin{aligned} y_1 &= a_1 r^m \sin m\theta + r(\tan\theta_0 \sin\theta + \cos\theta) + o(r) \\ y_2 &= a_2 r^m \sin m\theta + b_2 r^{n_2} \sin n_2\theta + o(r^{n_2}) \\ m &= \frac{\pi}{2\theta_0} \quad \pi/2 < \theta_0 < \pi \end{aligned} \tag{47a - c}$$

Equation (47a) shows that the 2nd order term of y_1 is given by $r(\tan\theta_0 \sin\theta + \cos\theta)$ instead of $r\cos\theta$. Since J depends on the combination of leading and 2nd order terms of y_1, we need to reevaluate J using (47a,b). A straightforward calculation using (47a,b) shows that the leading order behavior of J is

$$\begin{aligned} J &\sim m a_2 r^{m-1} \frac{\cos(\theta_0 - (1-m)\theta)}{\cos(\theta_0)} \equiv m a_2 r^{m-1} j(\theta) \\ m &= \frac{\pi}{2\theta_0} \end{aligned} \tag{48}$$

Note that J has the *same power law* singularity as in (33). However, although it is positive everywhere for $0 \leq \theta < \theta_0$, it vanishes at θ_0 since $m = \frac{\pi}{2\theta_0}$. The vanishing of J on the free edge implies that there is a boundary layer at $\theta = \theta_0$. The vanishing of J is important, because the traction free BC (24) and (27) relies on the assumption that the boundary terms associated with J were subdominant. This assumption is questionable if the asymptotic behavior of J at $\theta = \theta_0$ were unknown. The same issue was faced by Lenyel et al. (2014), who derived the near-tip fields for the special case of an interface crack where $\theta_0 = \pi$. In their work, they also found J vanishes at the crack face. They showed that J does not vanish at $\theta = \pi$ but has a different asymptotic behavior as $r \to 0$. Following the same line of reasoning [see Supporting information (SI)], we found a similar result where

$$J(r \to 0,\ \theta = \theta_0) = O\left(r^{-(1-m)/(1+\beta)}\right). \tag{49}$$

Substituting (49) into the traction free BC confirms that (24) and (27) is still valid, hence our leading order solution given by (47a,b) is still valid for all $\beta > 0$. However, the higher order terms in (47a,b) are only valid away from the boundary layer near the free edge. This claim is verified by the FE solution below.

4.3 Stresses

Using (47a,b), the components of the deformation gradient tensor, to leading order are

$$\begin{aligned} F_{11} &= a_1 m r^{m-1} \sin[(m-1)\theta],\ F_{12} = a_1 m r^{m-1} \cos[(m-1)\theta] \\ F_{21} &= a_2 m r^{m-1} \sin[(m-1)\theta], F_{22} = a_2 m r^{m-1} \cos[(m-1)\theta] \end{aligned} \tag{50a - d}$$

The leading asymptotic behavior of the *1st Piola stresses* can be evaluated using (7a–d) by ignoring the high order $J^{-2\beta-1}$ term and using (50a–d), this results in

$$\begin{aligned} P_{11} &= \mu a_1 m r^{m-1} \sin[(m-1)\theta], P_{12} = \mu a_1 m r^{m-1} \cos[(m+1)\theta] \\ P_{21} &= \mu a_2 m r^{m-1} \sin[(m+1)\theta], P_{22} = \mu a_2 m r^{m-1} \cos[(m-1)\theta] \end{aligned} \tag{51a - d}$$

The leading behavior of the *true stresses* are found using (8a-d), these are:

$$\begin{aligned} \tau_{11} &= \mu \frac{a_1^2 m r^{m-1}}{a_2 j(\theta)} \\ \tau_{12} = \tau_{21} &= \mu a_1 m r^{m-1}/j(\theta) \\ \tau_{22} &= \mu a_2 m r^{m-1}/j(\theta), \end{aligned} \tag{52a - c}$$

where $j(\theta)$ is defined by (48). Note angular variation of true stress is *identical for different stress components*. In particular, all stress components have the same power law singularity at the wedge tip, reflecting the mixed mode nature of the local fields. Analogous to stress intensity factors in fracture mechanics, the parameters a_1, a_2 uniquely characterize the strength of the singularity near the wedge tip. Equations (52a–c) imply that the ratio of different true stress components are *constants independent* of r and θ. Specifically,

$$\tau_{12}/\tau_{11} = \tau_{22}/\tau_{12} = a_2/a_1. \tag{53}$$

The ratio a_2/a_1 measures the ratio of interfacial shear stress to the transverse stress (τ_{11}) or the ratio of the normal stress to the shear stress respectively. In analogy to interfacial fracture mechanics, we define a phase angle ϕ_p

$$\phi_p \equiv \tan^{-1}(a_2/a_1) = \tan^{-1}(\tau_{12}/\tau_{11}) = \tan^{-1}(\tau_{22}/\tau_{12}). \tag{54a}$$

Equations (47a, b) provide another interpretation of phase angle, that is,

$$\lim_{r\to 0,\theta=\theta_0}(y_2/y_1) = a_2/a_1 \tag{54b}$$

Equation (54b) shows that *the free edge of the wedge near the tip deforms into a straight line with slope* given by the phase angle ϕ_p. It is important to note that the intensity factors a_α cannot be determined by asymptotic analysis since they depend on the manner of loading and specimen geometry. Therefore, the local slope of the deformed wedge depends on the applied load and the specimen geometry.

4.4 Deformed shape of the free edge

The asymptotic behavior (47a,b) states that at the free edge

$$y_1 \sim a_1 r^m - c(\theta_0)r, \text{ where } c(\theta_0) \equiv -(\tan\theta_0 \sin\theta_0 + \cos\theta_0) = -\sec\theta_0 > 0 \tag{55a}$$

$$y_2 \sim a_2 r^m \tag{55b}$$

Thus, the deformed free surface is locally described by the equation

$$y_1 = \frac{a_1}{a_2} y_2 - c(\theta_0)(y_2/a_2)^{1/m} \tag{55c}$$

The location of the maximum of y_1 is found by solving $dy_1/dy_2 = 0$, i.e.,

$$\frac{a_1}{a_2} = \frac{c(\theta_0)}{m}(y_2/a_2)^{1/m} y_2^{-1} \Rightarrow y_2 = [a_1 m\cos\theta_0]^{\frac{m}{1-m}} a_2 \tag{55d}$$

4.5 More higher order terms: William's expansion for nonlinear fields ($\pi \geq \theta_0 > \pi/2$)

Depending on β, we can generate additional higher order terms and obtain a William's type of expansion for nonlinear fields for wedge angle greater than 90°. Let

$$u_1 = a_1 r^m \sin m\theta + r\tan\theta_0 \sin\theta + r^{m_{12}} v_{12}(\theta) + o(r^{m_{12}})$$
$$y_2 = a_2 r^m \sin m\theta + a_{22} r^{m_{22}} \sin m_{22}\theta + r^{m_{23}} v_{23}(\theta) + o(r^{m_{23}}) \tag{56a, b}$$

where we have *modified notations* in (47a,b) so $b_2 = a_{22}$ and $m_{22} = n_2 = 3\pi/2\theta_0$. Also, $m_{12} > 1$ and $m_{23} \geq m_{22} = 3\pi/2\theta_0$. Substituting (56a,b) and (53) into the BC (15a) shows that

$$v'_{12}(\theta_0) = 0 \tag{57a}$$

provide that

$$m_{12} < 2\beta(1-m) + 1. \tag{57b}$$

Then it is easy to verify that the Laplacian term in (12a) is, to leading order

$$\nabla^2 u_1 \sim r^{m_{12}-2}\left(v''_{12} + m_{12}^2 v_{12}\right) \tag{58}$$

and is asymptotic dominant compared with the nonlinear term provided that (57b) is satisfied.

Equations (58) and (57a) and (13a) imply that

$$v_{12} = a_{12}\sin(m_{12}\theta), \text{ where } m_{12} = 3\pi/(2\theta_0) \tag{59}$$

Thus, the higher order terms depend on the value of β. Since we are interested in almost incompressible solids, β is typically very large so the condition (57b)

$$2\beta(1-m) + 1 > m_{12} = 3\pi/(2\theta_0) \tag{60}$$

is easily satisfied. Following the same line of reasoning we can determine m_{23} and $v_{23}(\theta)$ in (56b),

Indeed, we can continue this process to any positive integer $N \geq 2$ provided that

$$m_{\alpha N} < 2(1-m)\beta + 1, \quad \alpha = 1, 2 \tag{61}$$

The result is:

$$u_1 = a_1 r^m \sin m\theta + r\tan\theta_0 \sin\theta + \sum_{k=2}^{N} r^{m_{1k}} \sin(m_{1k}\theta) + o(r^{m_{1,N}})$$
$$y_2 = a_2 r^m \sin m\theta + \sum_{k=2}^{N} a_{2k} r^{m_{2k}} a_{2k} \sin(m_{2k}\theta) + o(r^{m_{2,N}}) \tag{62a, b}$$

where

$$m_{2k} = m_{1k} = \frac{(2k-1)\pi}{2\theta_0} \tag{62c}$$

Note the number of terms in the asymptotic series (62a,b) depend on β; specifically, this dependence is given by the inequality:

$$\frac{(2N-1)\pi}{2\theta_0} < 2\beta(1-m)+1. \tag{62d}$$

It should be noted that, unlike the William's expansion, which is an infinite series that converges within some radius of convergence at the crack tip; (62a,b) are asymptotic series, hence convergence is not guarantee, so including more terms of the series do not always lead to better accuracy.

5 Finite element results

5.1 Finite element (FE) calculations

We use FE to check our asympototic analyses. The geometry of the wedge structure and the FE model is shown in Fig. 4a and b. Calculations are performed using ABAQUS 2019. The bulk is modeled as a compressible Blatz–Ko material with energy density function given by (6). Calculations are performed using $\beta = 4.5$ which corresponds to $\nu = 0.45$. Let L be any arbitrary length scale, the specimen has a rectangular cross-section with sides $10L \times 11L$. On the top edge (BC), a uniform vertical displacement Δ is imposed while the horizontal shear traction is set to zero. The loading is controlled by the nominal stretch ratio $\lambda \equiv 1 + \frac{\Delta}{11L}$. On the line directly ahead of the wedge tip (OD), the vertical and horizontal displacements are set to zero to simulate perfect bonding with the rigid substrate. The wedge face AO is traction free. The sides AB and CD are free of shear traction and remain straight during deformation. Our choice of boundary conditions is similar to those used by Lenyel et al. (2014). This choice allows us to check our FE result against theirs for the special case of $\theta_0 = \pi$(interface crack). Following Lenyel et al. (2014), we use triangular elements for the entire mesh to prevent over-distortion of elements. Plane strain CPE6H elements are used. To balance the accuracy and efficiency of computation, we use a fine mesh near the wedge tip (the smallest element size is $\sim 1 \times 10^{-5}L$), while away from the tip the element size increases and is $\sim L/2$ near the top edge. Our convergence test shows that further refinement of the mesh does not affect the FE results.

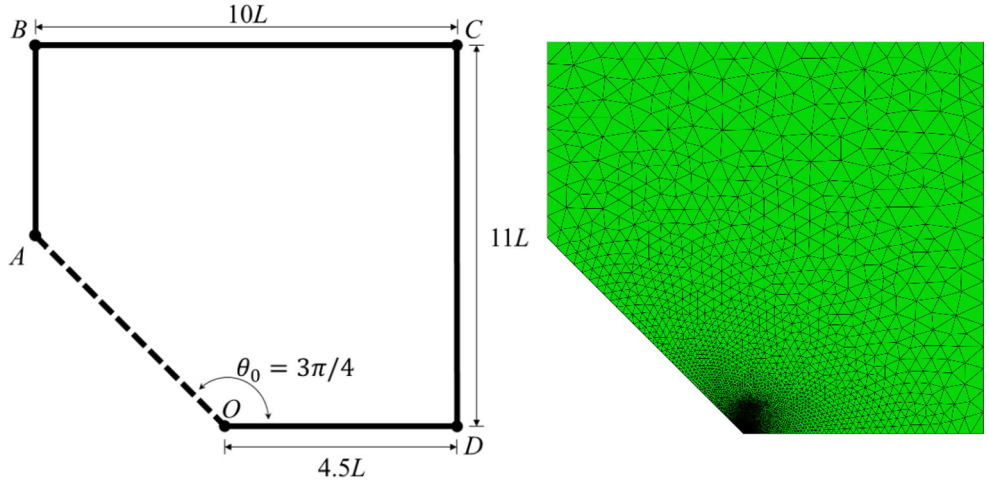

Fig. 4 (a, left) Wedge geometry in undeformed reference configuration, (b, right) Mesh used in FE calculation. A uniform vertical displacement Δ is applied on the edge BC while the edge OD is fixed to the rigid substrate. On AB the shear traction is zero. The wedge face AO is traction free. The sides AB and CD are free of shear traction and remain straight during deformation (this removes the stress concentration at the corners at A and D). In this geometry, the only loading parameter is the nominal stretch ratio $\lambda \equiv 1 + \frac{\Delta}{11L}$

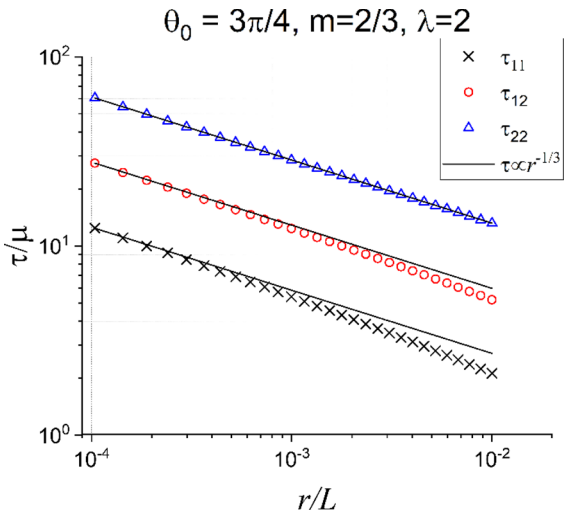

Fig. 5 Normalized true stresses on the interface $(\theta = 0)$ for a 135° wedge. Symbols are FE result, and the solid lines are the asymptotic results predicted by (52a–c)

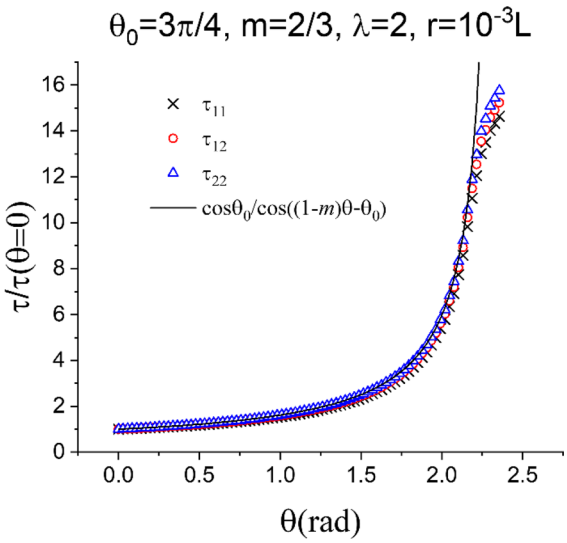

Fig. 6 Different components of the normalized true stress versus θ. Prediction of the asymptotic results given by (52a–c) are the solid lines

5.2 Comparison of FE results with asymptotic theory

We carried out simulations for various obtuse wedges $\theta_0 > \pi/2$ and for $\beta = 4.5$. Here we present results for $\theta_0 = 3\pi/4 = 135^0$. FE results for other values of θ_0 also validate our asymptotic results and are given in the S3. Figure 5 shows that true stresses on the interface $(\theta = 0)$ versus distance from the wedge tip.

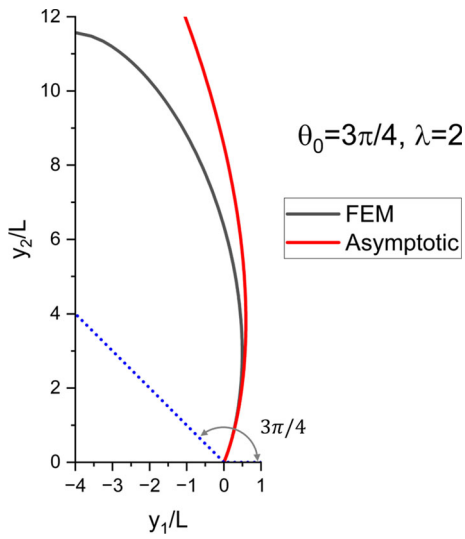

Fig. 7 Deformed shape of the free edge. Black solid line is the FE result and red solid line is the asymptotic result (55c). The undeformed wedge surface (with angle $\theta_0 = 3\pi/4$) is the dotted line

The asymptotic results (52a–c) (solid lines with slope $-1/3$ in a log–log plot) are also plotted for comparison. The FE and asymptotic results are in good agreement for $r/L < 10^{-3}$.

To check the angular dependence of the true stresses we plot normalized FE true stress components $\overline{\tau}_{\alpha\beta} \equiv \tau_{\alpha\beta}(r/L = 10^{-3}, \theta)/\tau_{\alpha\beta}(r/L = 10^{-3}, \theta = 0)$ in Fig. 6. If our asymptotic results (52a–c) are correct, then different components of $\overline{\tau}_{\alpha\beta}$ should coincide with $1/j(\theta)$. Figure 6 shows that this is indeed the case except for a boundary layer at θ_0 where $j(\theta_0) = 0$. As noted earlier, the existence of this boundary layer is expected [see discussion right after (48)]. The deformed shape of the free edge obtained from FE is shown in Fig. 7. Plotted in the same figure is the asymptotic result (55c). Again, there is good agreement between theory and FE results.

6 Special case: 90° wedge

6.1 Shallow wedges: $0 < \theta_0 \leq \pi/2$

We call wedges with angles less than or equal to 90 degrees shallow wedges. For these wedges, our analysis indicates that the stresses cannot have a power singularity. Of course, this result does not

prevent the stresses having a weaker singularity (e.g., a logarithmic singularity in r). Here we focus on the border-line case where $\theta_0 = \pi/2$. This case appears often in applications, since many structures have 90° corners. Another reason to study this case is that we expect wedges with angles smaller than 90° will have weaker singularities, if they exist at all.

6.2 Results for 90° wedge

The structure of the asymptotic fields near the corner turns out to be very difficult to analyze and we have not been able to obtain exact results. For this reason, we first present FE results. These FE results provide valuable insight on the near wedge tip fields. Based on these results, we obtain approximate close form expressions for the true stresses near the wedge tip. The FE geometry is a square with sides $10L$. The boundary conditions are the same as $\theta_0 > \pi/2$.

The normalized true stresses $\tau_{\alpha\omega}/\mu$ along the interface $(\theta = 0)$ versus distance r from the wedge tip for two different applied stretch ratios $\lambda = 1.5, 5.0$ are plotted in Fig. 8a, b. As shown in Fig. 8a, b, these FE results (symbols) of near tip stress components can be well approximated by

$$\begin{aligned} \tau_{11}/\mu &= B_1(\ln r)^2 + C_1 \ln r + D_1 \\ \tau_{12}/\mu &= C_2 \ln r + D_2 \\ \tau_{22}/\mu &= D_3 \end{aligned} \qquad (63a-c)$$

The dimensionless parameters B_i, C_i and D_i in (63a–c) are functions of θ and the applied stretch ratio λ.

To study the angular variation of B_i, C_i, D_i we evaluate the true stresses on $\theta = \pi/2$. On this edge, the traction free condition implies that (see SI)

$$\tau_{11}\tau_{22} = \tau_{12}^2 \quad \theta = \pi/2 \qquad (64)$$

We also confirmed (64) using our FE calculation. Equation (64) implies that B_i, C_i, D_i are not independent. Another way to see this is that stresses must satisfy equilibrium. Figures 9a, b plot the true stress along $\theta = \pi/2$ for two different applied stretches. The asymptotic results given by (63a–c) are plotted in the same figure as a comparison. Again, the agreement between FE and (63a–c) is excellent. These results strongly support the validity of (63a–c) for all angles. Results for true stress along $\theta = \pi/6, \pi/3$ are given in Supporting Information.

The deformed shapes of the free edge are shown in Fig. 10 for $\lambda = 1.5$, 2 and 5. It is interesting to note

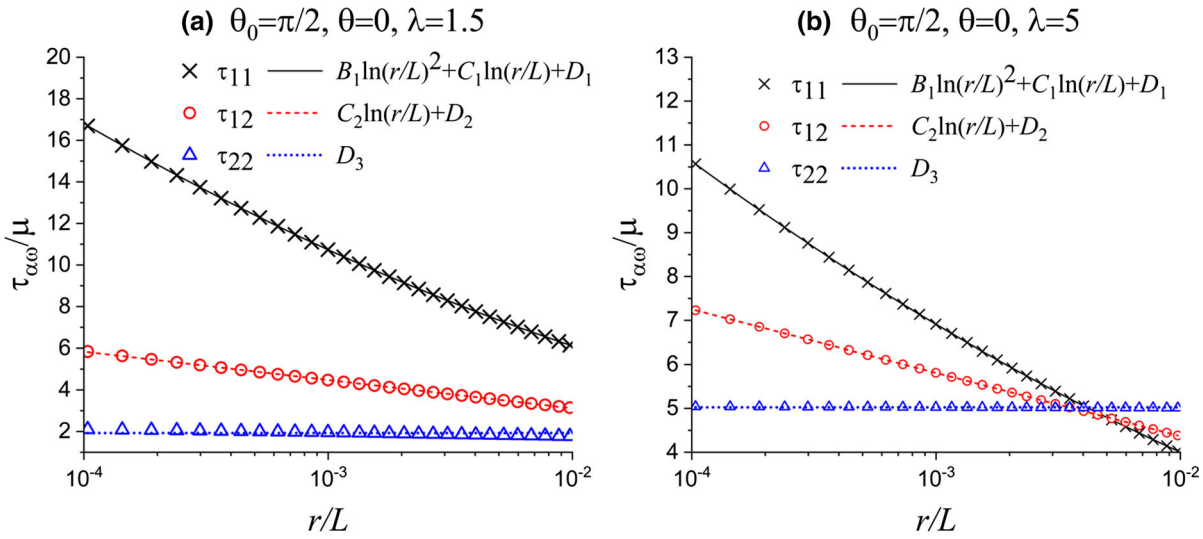

	B_1	C_1	D_1	C_2	D_2	D_3
Fig. 8(a)	0.136	−0.445	1.17	−0.592	0.386	1.92
Fig. 8(b)	0.0764	−0.383	0.620	−0.627	1.48	5.02

Fig. 8 True stress components directly ahead of wedge tip $(\theta = 0)$ for a 90 degrees wedge. **a** (left), $\lambda = 1.5$, β = 4.5. **b** (right),$\lambda = 5$, β = 4.5. Symbols are FE results and solid lines are Eq. (63a–c)

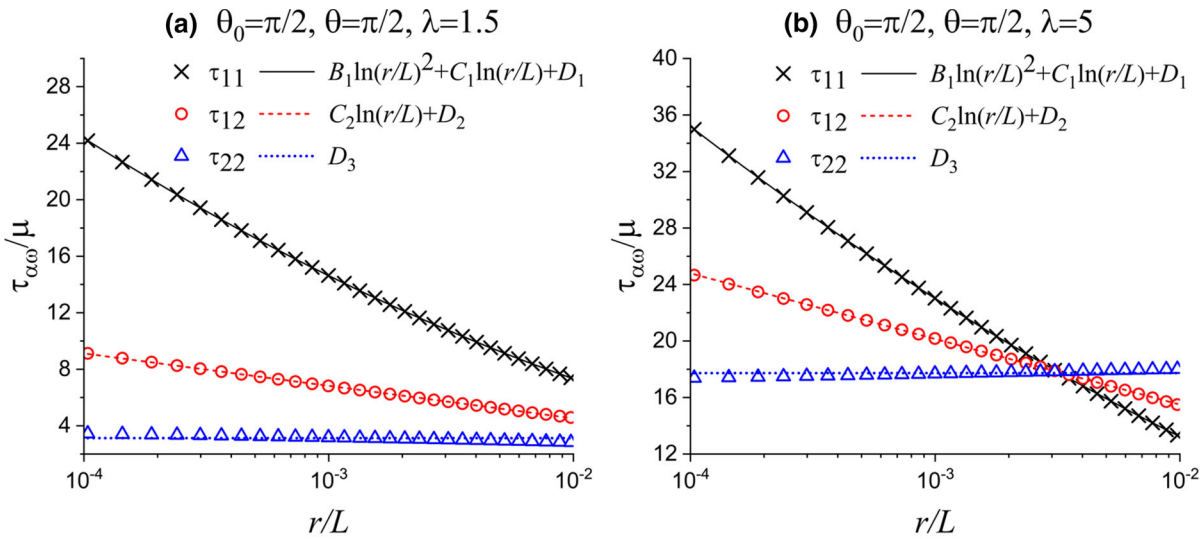

	B_1	C_1	D_1	C_2	D_2	D_3
Fig. 9(a)	0.230	−0.527	0.0304	−0.998	−0.0653	3.12
Fig. 9(b)	0.226	−1.65	0.848	−2.02	6.20	17.7

Fig. 9 True stress distribution along the free edge for β = 4.5. $\lambda = 1.5$(**a**, left). $\lambda = 5$ (**b**, right). Symbols are FE results and solid lines are Eq. (63a–c)

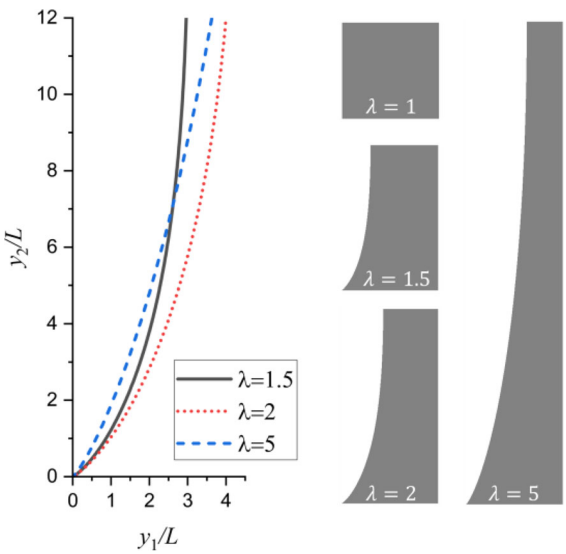

Fig. 10 Finite element results for the deformed shape of the free edge near the tip of a 90 degrees wedge for $\beta = 4.5$. The applied stretch ratios are $\lambda = 1.5$, 2.0 and 5.0. *Local* deformed shapes with origin at the wedge tip (left). Right figure shows the reference configuration ($\lambda = 1$) and the deformed shapes

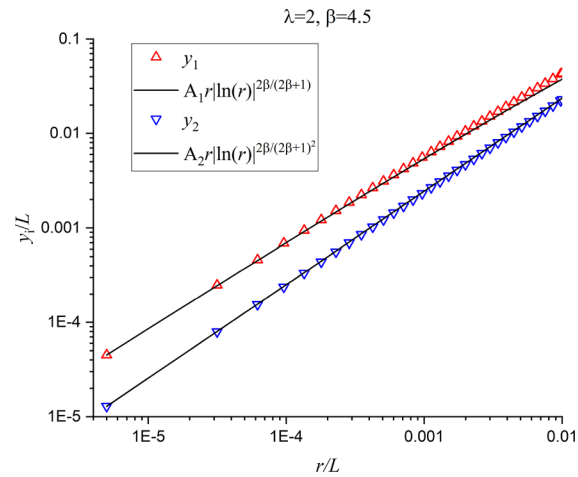

Fig. 11 Deformed coordinates $y_i (i = 1, 2)$ versus normalized distance along the free edge ($\theta = \pi/2$). The symbols are FE results, and the solid lines are the asymptotic expressions (65a,b)

that the local wedge shape is not a monotonic function of the applied stretch. Up till $\lambda \approx 2$, the lateral surface contraction increases. This trend is reversed at large stretch ratio, e.g., $\lambda = 5$. This behavior is due to finite compressibility.

Figure 11 plots the asymptotic behavior of y_1 and y_2 on $\theta = \pi/2$, that is, the local deformed coordinates of the wedge surface. This figure shows that the expressions

$$y_1 \sim A_1 r\left[(\ln r)^2\right]^{\frac{\beta}{2\beta+1}}$$
$$y_2 \sim A_2 r\left[(\ln r)^2\right]^{\frac{\beta}{(2\beta+1)^2}}, \quad (65a, b)$$

provide a good fit to the FE result. In (65a,b), A_1 and A_2 are dimensionless parameters that depend on λ and θ.

Here we note that (65a,b) imply that

$$\frac{y_2}{y_1} \sim \frac{A_2}{A_1}\left[(\ln r)^{-2}\right]^{\frac{2\beta}{(2\beta+1)^2}} \quad (66)$$

Thus, the local slope vanishes at the wedge tip (recall that this local slope is always positive for an obtuse wedge).

7 Summary and discussion

A finite strain model based on a compressible Blatz–Ko model is used to study the plane strain deformation field near the tip of wedges with internal angles $\theta_0 \in (0, \pi)$. For reentrant corners where $\theta_0 > \pi/2$, the true stresses (as well as the 1st Piola stress) as the wedge tip is approached have a power law singularity of the form r^{m-1} where $m = \frac{\pi}{2\theta_0}$. Our asymptotic analysis is confirmed by FE calculations. The magnitude of these wedge tip fields are controlled by two loading parameters, a_1 and a_2, analogous to mixed mode stress intensity factors in linear elastic fracture mechanics. Specifically, the ratio a_2/a_1 measures the ratio of interfacial shear stress to the transverse stress (τ_{11}) or the ratio of the normal stress to the shear stress respectively. An interesting result is that the local deformed shape of the wedge is a straight line with slope determined by a_2/a_1. Hence, the wedge in the reference configuration is mapped to another wedge in the deformed configuration. A surprising result is that the leading asymptotic behavior is *independent of the small strain Poisson's ratio or* β, in contrast to small strain theory (see Fig. 2). Furthermore, for a given wedge angle $\theta_0 \in (\pi/2, \pi)$, the singularity index is larger than the singularity index predicted by the linear theory. *As a result, the stress singularity predicted by the nonlinear theory is less severe.* Note this is not always true, for example, for a Mode *I* crack in a homogenous neo-Hookean incompressible solid, the opening component of the true stress directly ahead of the crack tip has a higher singularity than that predicted by linear theory (Long and Hui 2015). In addition, the singular stress fields in the nonlinear theory have no oscillation. This result is consistent with Knowles and Sternberg (1983), who show that the stress field of an interface crack between two different neo-Hookean sheets does not have infinite oscillations. For sufficiently low compressibility or large β, we obtain higher order terms of the asymptotic series—analogous to William's expansion in linear theory.

In contrast to the linear theory, we find no power law singularity when $\theta_0 \in (\pi/4, \pi/2]$. Instead, we found a transition in asymptotic behavior at $\theta_0 = \pi/2$. For a 90-degree wedge, numerical result shows that the power law singularity of the true stresses is replaced by a much weaker logarithmic singularity. Although we cannot provide a rigorous proof that no singularity exists for $\theta_0 < \pi/2$; such a singularity, if it exists, will be extremely weak for these angles. An interesting result is that the local deformed shape of the 90° wedge has zero slope [see (66)]. These departures from LEFM offer important insights into the limitations of small strain theory; they lead to better understanding of soft material failure and can serve as a useful tool aiding the interpretation of experiments. For example, our theory indicates that design of fibril tip architecture based on linear elastic wedge theory is conservative which increases the safety factor and can lead to more reliable reusable adhesives.

There are obvious limitations to our theory. Our asymptotic result is for the Blatz–Ko model. A difficulty with large deformation theory is that asymptotic results are constitutive model dependent. This means that if we use a different compressible model, the asymptotic result will be different. Furthermore, there is no proof that the limit where $\beta \to \infty$ in our solution corresponds to a neo-Hookean *incompressible* solid.

Acknowledgements C.Y. Hui and B. Zhu are supported by the National Science Foundation under Grant No. CMMI-1903308.

Declarations

Conflict of interest The authors declare that they have no known competing financial interests or personal relationships that could have appeared to influence the work reported in this paper.

References

Aksak B, Sahin K, Sitti M (2014) The optimal shape of elastomer mushroom-like fibers for high and robust adhesion. Beilstein J Nanotechnol 5:630–638. https://doi.org/10.3762/bjnano.5.74

Arzt E, Gorb S, Spolenak R (2003) From micro to nano contacts in biological attachment devices. Proc Natl Acad Sci 100(19):10603–10606. https://doi.org/10.1073/PNAS.1534701100

Blatz PJ, Ko WL (1962) Application of finite elastic theory to the deformation of rubbery materials. Trans Soc Rheol 6(1):223–252. https://doi.org/10.1122/1.548937

Bogy DB (1968) Edge-bonded dissimilar orthogonal elastic wedges under normal and shear loading. J Appl Mech 35(3):460–466. https://doi.org/10.1115/1.3601236

del Campo A, Greiner C, Arzt E (2007) Contact shape controls adhesion of bioinspired fibrillar surfaces. Langmuir 23(20):10235–10243. https://doi.org/10.1021/la7010502

Dempsey JP, Sinclair GB (1979) On the stress singularities in the plane elasticity of the composite wedge. J Elast 9(4):373–391. https://doi.org/10.1007/BF00044615

Dunn ML et al (1997a) Fracture initiation at sharp notches under mode I, mode II, and mild mixed mode loading. Int J Fract 84:367–381. https://doi.org/10.1023/A:1007346203407

Dunn ML, Suwito W, Cunningham S (1997b) Fracture initiation at sharp notches: correlation using critical stress intensities. Int J Solids Struct 34(29):3873–3883. https://doi.org/10.1016/S0020-7683(96)00236-3

England AH (1965) A crack between dissimilar media. J Appl Mech 32(2):400–402. https://doi.org/10.1115/1.3625813

Gao YC (1990) Elastostatic crack tip behavior for a rubber-like material. Theoret Appl Fract Mech 14(3):219–231. https://doi.org/10.1016/0167-8442(90)90021-Q

Geubelle PH, Knauss WG (1994a) Finite strains at the tip of a crack in a sheet of hyperelastic material: I. Homogeneous case. J Elast 35(1–3):61–98. https://doi.org/10.1007/BF00115539

Geubelle PH, Knauss WG (1994b) Finite strains at the tip of a crack in a sheet of hyperelastic material: II. Special bimaterial cases. J Elast 35(1–3):99–137. https://doi.org/10.1007/BF00115540

Geubelle PH, Knauss WG (1994c) Finite strains at the tip of a crack in a sheet of hyperelastic material: III. General bimaterial case. J Elast 35(1–3):139–174. https://doi.org/10.1007/BF00115541

Gorb S et al (2006) Biomimetic mushroom-shaped fibrillar adhesive microstructure. J R Soc Interface 4(13):271–275. https://doi.org/10.1098/RSIF.2006.0164

Hein VL, Erdogan F (1971) Stress singularities in a two-material wedge. Int J Fract Mech 7(3):317–330. https://doi.org/10.1007/BF00184307

Jagota A, Hui CY (2011) Adhesion, friction, and compliance of bio-mimetic and bio-inspired structured interfaces. Mater Sci Eng R 72(12):253–292. https://doi.org/10.1016/J.MSER.2011.08.001

Kim S, Sitti M (2006) Biologically inspired polymer microfibers with spatulate tips as repeatable fibrillar adhesives. Appl Phys Lett 89(26):261911. https://doi.org/10.1063/1.2424442

Knowles JK, Sternberg E (1973) An asymptotic finite-deformation analysis of the elastostatic field near the tip of a crack. J Elast 3(2):67–107. https://doi.org/10.1007/BF00045816

Knowles JK, Sternberg E (1974) Finite-deformation analysis of the elastostatic field near the tip of a crack: reconsideration and higher-order results. J Elast 4(3):201–233. https://doi.org/10.1007/BF00049265

Knowles JK, Sternberg E (1983) Large deformations near a tip of an interface-crack between two Neo-Hookean sheets. J Elast 13(3):257–293. https://doi.org/10.1007/BF00042997

Leguillon D (2002) Strength or toughness? A criterion for crack onset at a notch. Eur J Mech A Solids 21:61–72. https://doi.org/10.1016/S0997-7538(01)01184-6

Lengyel TH, Long R, Schiavone P (2014) Effect of interfacial slippage on the near-tip fields of an interface crack between a soft elastomer and a rigid substrate. Proc R Soc A. https://doi.org/10.1098/rspa.2014.0497

Long R, Hui CY (2015) Crack tip fields in soft elastic solids subjected to large quasi-static deformation—a review. Extreme Mech Lett 4:131–155. https://doi.org/10.1016/J.EML.2015.06.002

Mansouri K et al (2016) Singular elastostatic fields near the notch vertex of a Mooney–Rivlin hyperelastic body. Int J Solids Struct 80:532–544. https://doi.org/10.1016/J.IJSOLSTR.2015.10.013

Marques EAS, da Silva LFM (2008) Joint strength optimization of adhesively bonded patches. J Adhes 84(11):915–934. https://doi.org/10.1080/00218460802505275

Müller A, Wapler MC, Wallrabe U (2019) A quick and accurate method to determine the Poisson's ratio and the coefficient of thermal expansion of PDMS. Soft Matter 15:779–784. https://doi.org/10.1039/c8sm02105h

Muskhelishvili NI (1977) Some basic problems of the mathematical theory of elasticity. Noordhoff, Groningen

Ornes S (2013) Mussels' sticky feet lead to applications. Proc Natl Acad Sci USA 110(42):16697–16699. https://doi.org/10.1073/PNAS.1317104110

Rice JR, Sih GC (1965) Plane problems of cracks in dissimilar media. J Appl Mech 32(2):418–423. https://doi.org/10.1115/1.3625816

Spuskanyuk A et al (2008) The effect of shape on the adhesion of fibrillar surfaces. Acta Biomater 4(6):1669–1676. https://doi.org/10.1016/J.ACTBIO.2008.05.026

Stephenson RA (1982) The equilibrium field near the tip of a crack for finite plane strain of incompressible elastic materials. J Elast 12(1):65–99. https://doi.org/10.1007/BF00043706

Tramacere F et al (2014) Structure and mechanical properties of *Octopus vulgaris* suckers. J R Soc Interface. https://doi.org/10.1098/RSIF.2013.0816

Williams ML (1952) Stress singularities resulting from various boundary conditions in angular corners of plates in extension. J Appl Mech 19(4):526–528. https://doi.org/10.1115/1.2791085